CONTENTS

CHAPTER 2

THE GAURIBIDANUR RADIO TELESCOPE (GEETEE)

Chapter 2

THE GAURIBIDANUR RADIO TELESCOPE (GEETEE)

The telescope with which the observations described in this thesis were made is situated near Gauribidanur (longitude $77^{\circ}\ 26'\ 07''$ E; latitude $13^{\circ}\ 36'\ 12''$ N), about 80 km north of Bangalore, India. The telescope, in the shape of the letter T, is made of 1000 dipoles with a 1.4 km long East-West arm and 0.45 km long Southern arm. This chapter is devoted to a description of the telescope. Sections 2.1 and 2.2 give details of the antenna and the receiver system. Section 2.3 and 2.4 discuss the performance of the receiver and the antenna respectively. A brief discussion of the sensitivity to be expected in the present survey is presented in Section 2.5. Section 2.6 deals with the grating response of the array.

2.1 THE ANTENNA

2.1.1 The basic unit

The smallest unit of the antenna system is the fat dipole which is shown schematically in figure 2.1. For brevity we shall hereafter refer to it as simply the "dipole". The length of the dipole, its height above the reflector wire and the separation between each of the component wires were adjusted to operate with a resonable standing wave ratio in the range of frequencies between 25 MHz and 35 MHz.

The far-field pattern of the dipole in the plane perpendicular to the axis of the dipole is theoretically expected to be

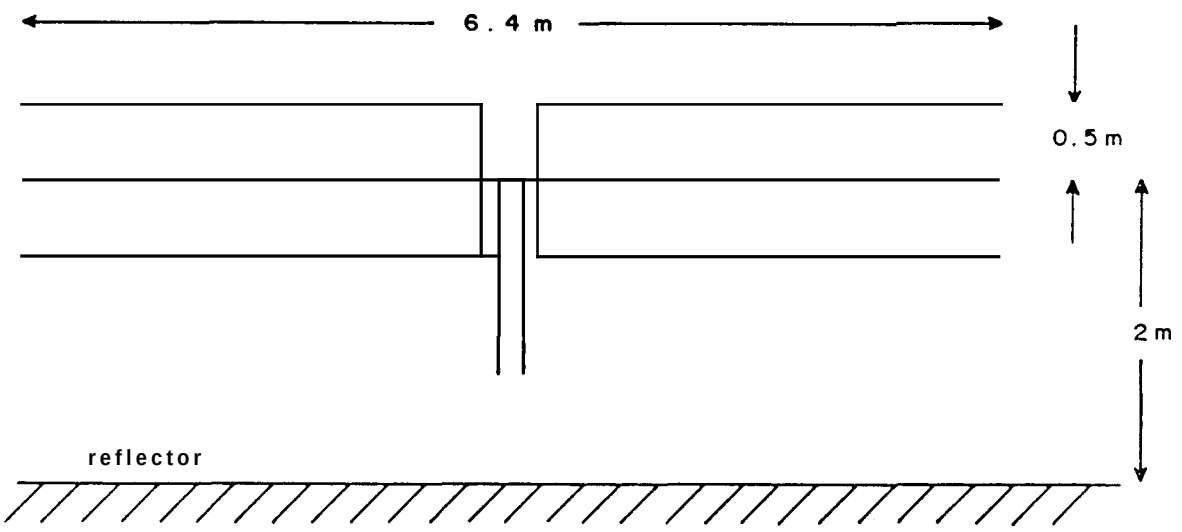

Fig. 2.1: The fat dipole

Characteristic impedance : 600 Ω
Bandwidth : 25–35 MHz with a VSWR of 1.1–1.5
Polarisation : linear, oriented along EW

$$V(\theta) \propto \sin\left(\frac{2\pi}{\lambda} H \cos(\theta)\right) \qquad (2.1)$$

where θ is the angle from zenith and H is the height of the centre of the dipole above the reflector wire. This comes from combining the dipole and its image in the reflector plane. The dipole without the reflector wire is assumed to have an isotropic radiation pattern in the plane parpendicular to its axis. These dipoles are designed to have a standard collecting area of $0.25\lambda^2$ where λ is the wavelength of observation. In the present case this is ≈ 19 q^2 corresponding to $\lambda = 8.69$ m. We will return to these matters in the next chapter when we discuss calibration and flux scales.

The dipoles are oriented East-West (EW) and are spaced 8.6 m apart in this direction. They accept linear polarisation.

Four dipoles along the EW direction are combined through open-wire transmission lines and appropriate impedance transformers to form a basic unit (Fig. 2.2).

2.1.2 The East-West **and** Southern arrays

The East-West array consists of 4 rows of dipoles s'paced 5 m apart in the north-south (NS) direction as shown in figure **2.3(a).** Dipoles in the array are combined further in the Christmas tree fashion as shown'in figures **2.3(b)** and 2.4 to produce the East and the West outputs which are brought to the laboratory separately. The EW array has a collecting area **$\approx$12000 m^2.**

The Southern (S) array consists of 90 basic units placed **5** m apart along the NS direction (Fig. 2.3(a)). Each of the basic

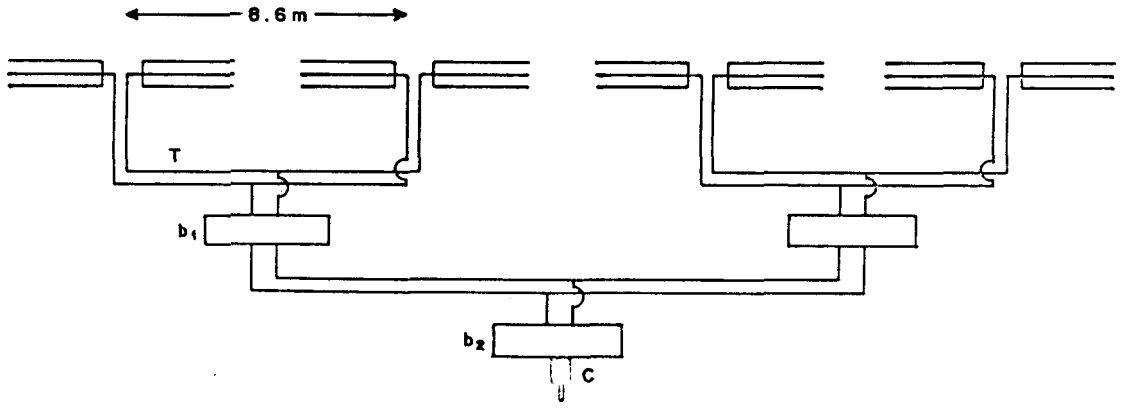

T : An open-wire transmission line of 600 Ω characteristic impedance. It has a loss of 0.2 dB/100 m. The measured phase change is less than 1^{o} for a temperature variation from 25 C to 35 C.

b_1 : A balance to balance impedance transformer (300 Ω to 600 Ω) with an insertion loss less than 0.2 dB.

b_2 : A balance to unbalance impedance transformer (600 Ω to 50 Ω). It has an insertion loss of 0.5 dB.

C : A co-axial cable (RG 58U) with an insertion loss of 10 dB/100 m.

Fig. 2.2: The basic unit

A view of the West array as seen from the centre of the East-West array.

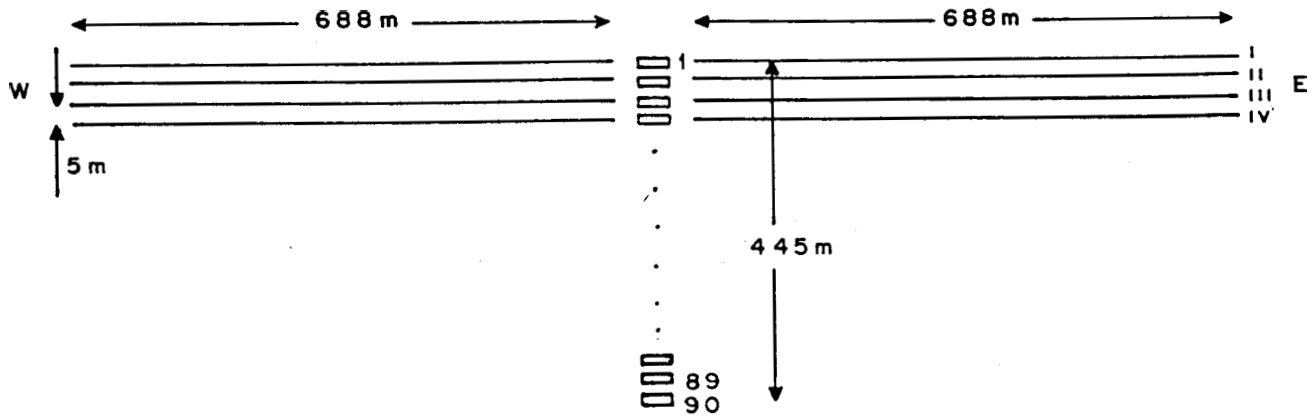

Fig. 2.3(a): The Gauribidanur radio telescope (GEETEE)

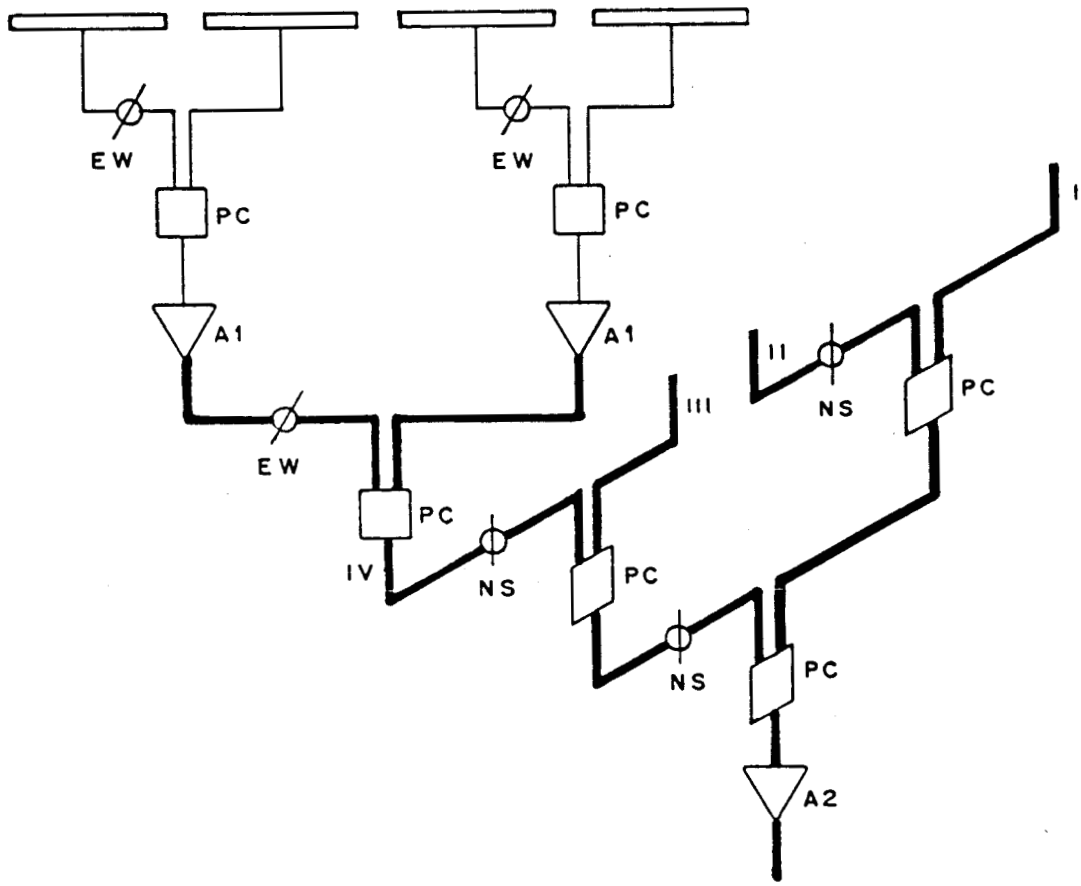

Fig. 2.3(b): The Christmas tree configuration in the EW array consisting of 4 basic units is shown in detail. The outputs of the basic units are carried further through co-axial cables and are added in power combiners (PC). The thin lines indicate RG 58U (50Ω) cables while the thicker lines indicate RG 8U (50Ω) cables. A1 and A2 are F.E.T. amplifiers and cascade amplifiers respectively.

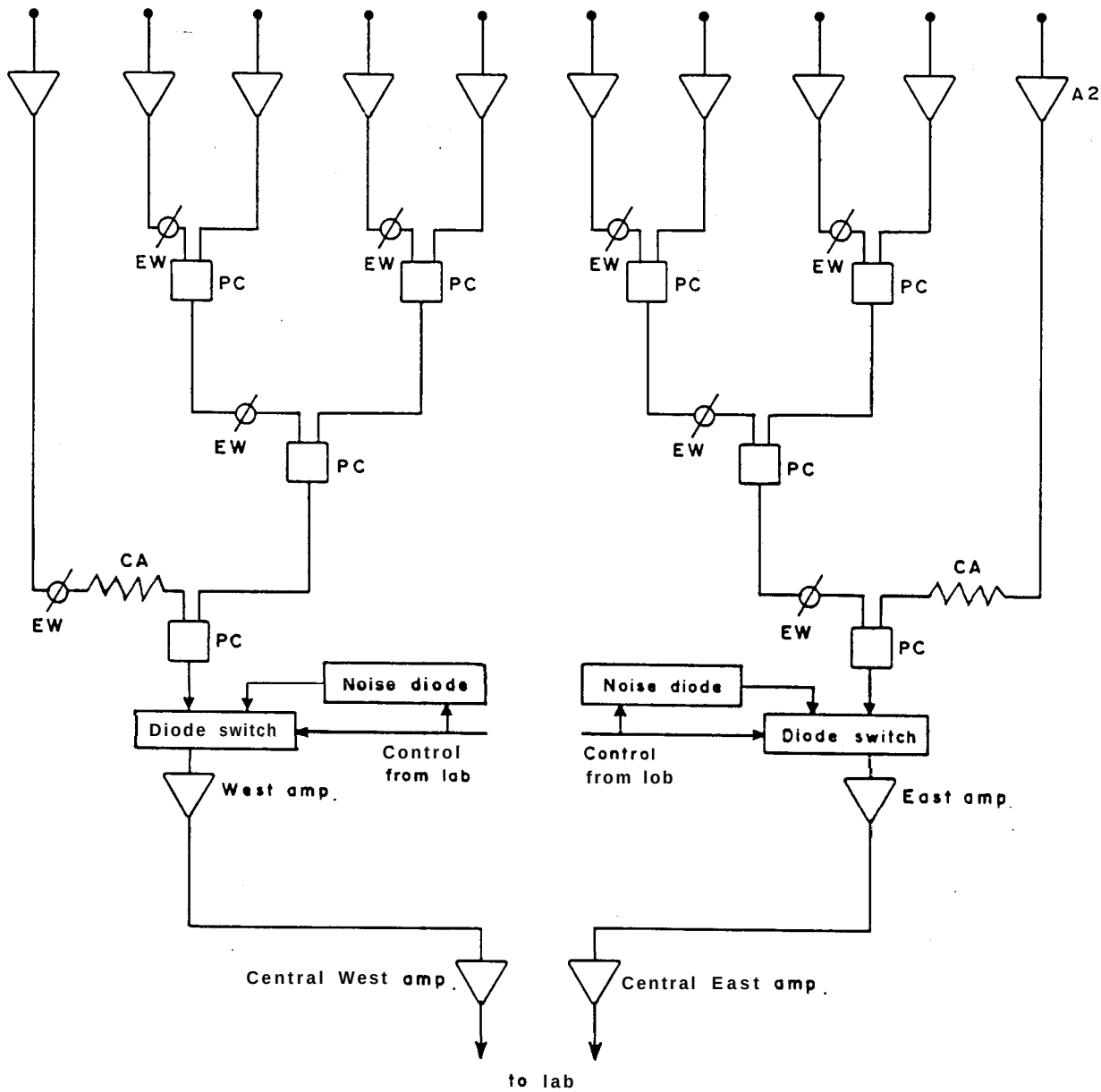

Fig. 2.4: This illustrates the signal path in the EW array subsequent to the output stage of the amplifier **A2.** There are 10 such units in the array. Two outputs each consisting of the combined output of 5 units are brought to the laboratory. The purpose of the noise diode and the switch is to monitor the gains of the subsequent part of the Christmas tree. The symbol 'CA' refers to 'compensating attenuator' and 'PC' to 'power combiner'.

units has a pre-amplifier following it. The signals from the basic units are brought to the laboratory through open-wire transmission lines. The S array has a collecting area $\approx 7000\ m^2$.

For the purpose of making the sky survey we use one of the rows of the EW array in the transit mode and measure the visibilities corresponding to the various baselines which it forms with respect to the basic units of the S array. Any one row of the EW array as well as each of the S array basic units have primary beams which are essentially looking at the whole sky along NS (eq. 2.1, **i.e.** along the meridian. By fourier transforming the visibilities along the NS the brightness distribution of the sky along NS at that instant of time can be obtained. Since ther are **90** basic units in the **S** array we need to measure **90** visibilities. The receiver system, however, has only 32 front ends. Hence, a time multiplexing between the signals from the S array basic units is required. In the present scheme, this was achieved by installing 23 sets of diode switches - one set each for a set of 4 basic units in the S array (Fig. 2.5). The signal from each basic unit in the southern array is power split after the preamplifier. One output is used in the single beam forming network while the other is used for the synthesis observations described in this thesis. Four outputs from 4 basic units come to the diode switch box. Control signals to this box come from the lab and select one unit at a time - the cycle time being ≈ 1 **sec.** In EW only one out of the 4 rows has to be chosen. Row I and Row **IV** were considered inappropriate since they see a more asymmetric environment. Either row **II** or **III** is better suited. We chose row **III** for our observations

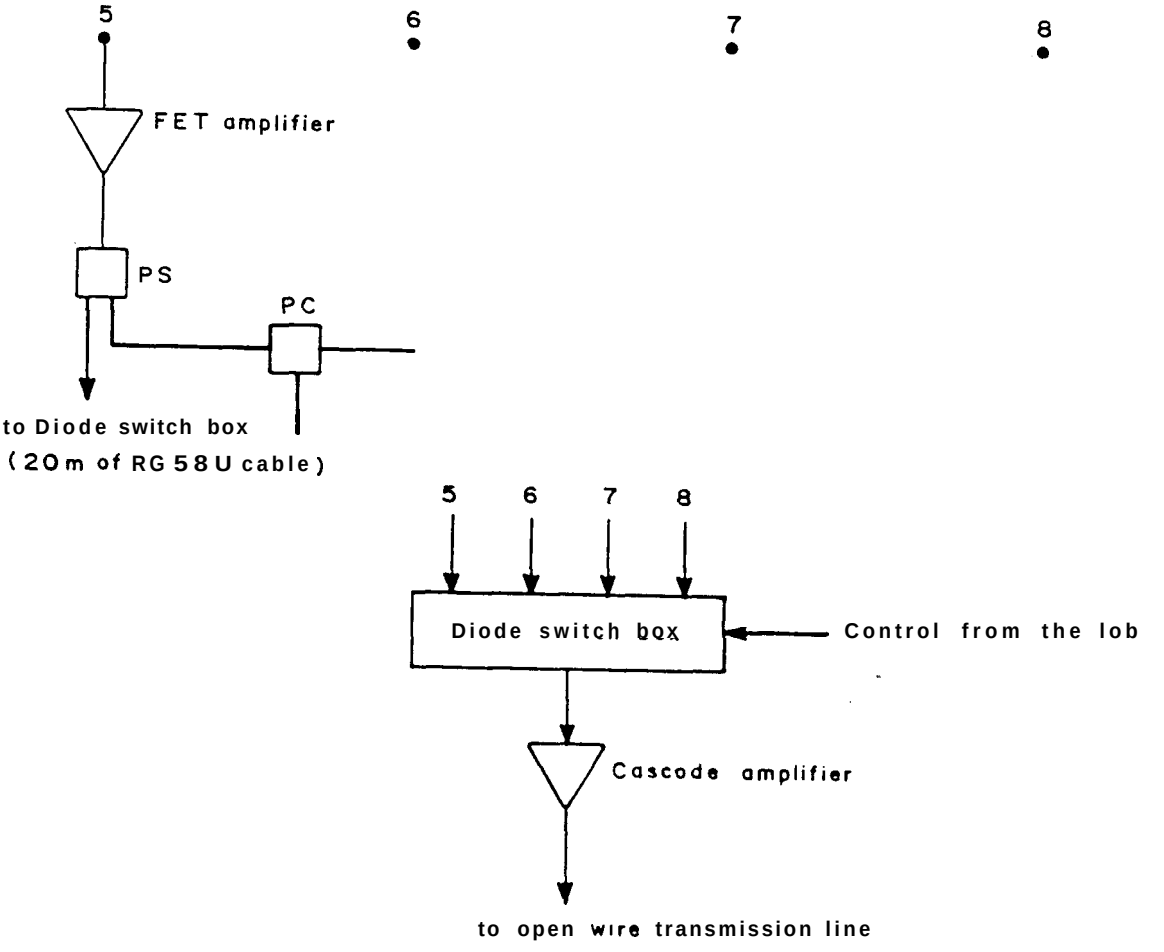

Fig. 2.5: Configuration used in the S-array for the sky survey. Numbers 5,6,7 and 8 refer to the basic units in the S-array. Time multiplexing between every 4 units in the S-array was adopted for the purpose of the survey. PS and PC refer to power splitter and power combiner respectively.

(Figs. 2.3(a) and 2.6(a)).

Field effect transistors are used in all the pre-amplifiers in the EW and S arrays. These amplifiers have a gain of $\approx$6 dB at 34.5 MHz, and a bandwidth at half power of $\pm$ 2 MHz. They have a noise temperature of $\approx$500 K and very low intermodulation distortion,

2.1.3 The zero spacing

One of the important objective of the present survey is to map the Galactic background radiation and be able to give the brightness temperature of any part of the sky unambiguously. This is possible if the antenna system responds to all angular scale structures (larger than its resolution) in the sky. With this in view we have included in our observation all spacings and in particular the zero spacing also. Figure 2.6(b) shows the configuration of the antenna adopted to include the zero spacing. The output from the 3rd basic unit in the S array (S_3), which is in line with the III row of the EW array, is added to the EW array appropriately. The visibility resulting from the multiplication of the signals from the EW array and S_3 now corresponds to the zero baseline. The noise due to the F.E.T. amplifier in S_3 which is common to both the EW array and S_3 contributes $\approx$ 500 K to the signal from the sky in the zero spacing. Since the brightness temperature of the sky at frequencies around 30 MHz is $\gtrsim 10^4$ K, this leads to a small offset in the estimation of the brightness temperature of the sky.

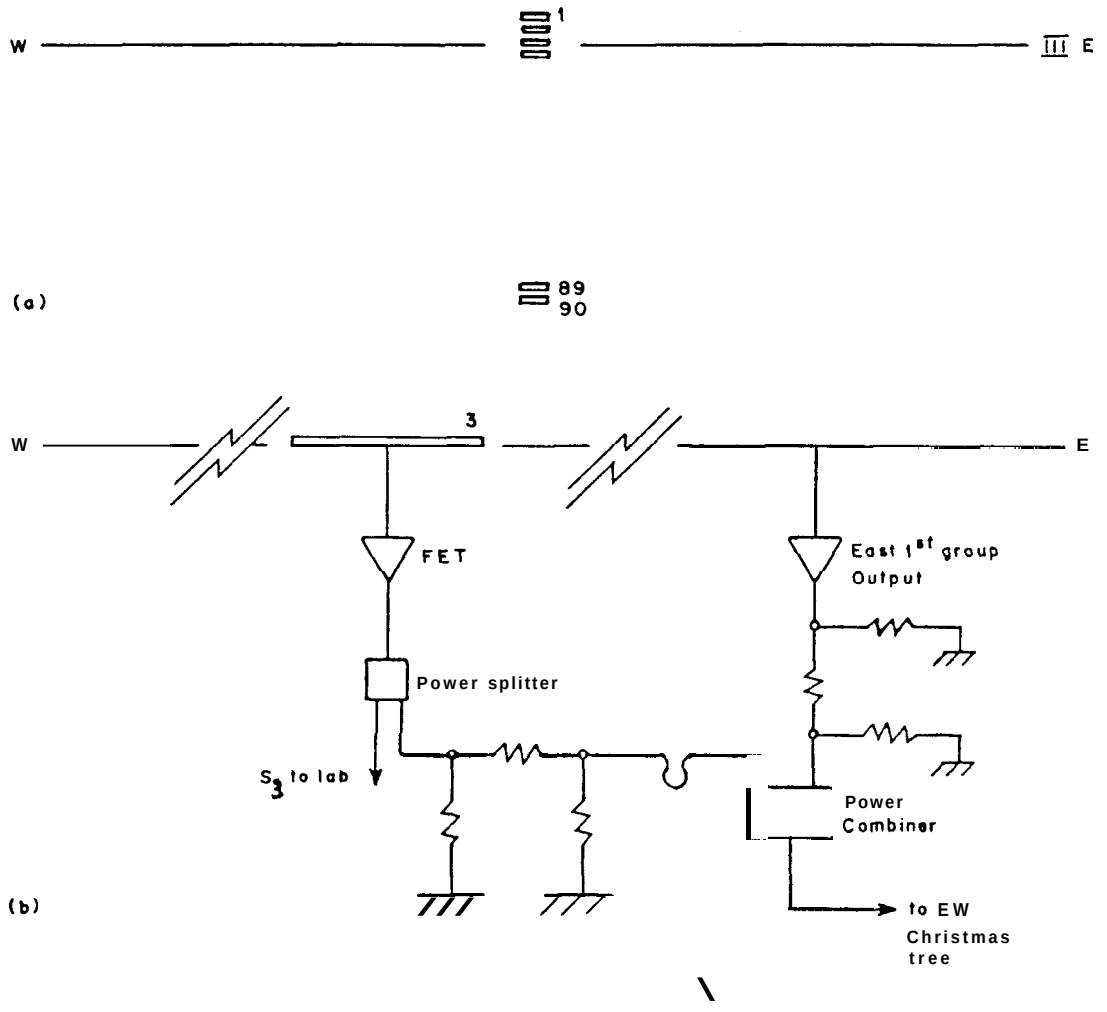

Fig. 2.6(a): This shows the final antenna configuration used for the sky survey. Only one row of the EW array is used. Numbers marked along the S-array refer to the basic units in the array.

Fig. 2.6(b): This illustrates the inclusion of the zero spacing. The third basic unit of the S-array (S_3) which is in line with the III row of the EW array is made part of that row also. Multiplication of the III row of EW with S_3 corresponds to zero spacing.

2.2 THE RECEIVER SYSTEM

A complete description of the receiver system can be found in an earlier thesis (Udayashankar,N. 1986). Here, we highlight only the concepts.

Figure 2.7 shows the block diagram of the scheme used to obtain any one of the visibilities.

The receiver employs a one-bit correlator system. In this scheme the input signals are infinitely clipped and their zero cross overs measured in a zero cross detector (Fig. 2.7). One-bit correlators measure the normalised correlation coefficient. The amplitude information of the signal is lost. If a correlation ρ_m is obtained by infinitely clipping (i.e. one-bitting) the two signals which are band limited and Gaussian in nature then the normalised correlation coefficient ρ_c is given by,

$$\rho_c = \sin\left(\frac{\pi}{2}\rho_m\right) \qquad (2.2)$$

(van Vleck and Middleton 1966) and ρ_c is related to the analog correlation ρ_a by,

$$\rho_a = \sigma_1 \sigma_2 \rho_c \qquad (2.3)$$

where σ_1 and σ_2 are the r.m.s. values of the two signals being multiplied. In this case the two signals correspond to the EW signal and the signal from any Southern element. Their amplitudes are continuously recorded to obtain σ_1 and σ_2.

A novel method using a hardware scheme similar to that used in the one-bit correlators (Udayashankar, N. 1986) has been

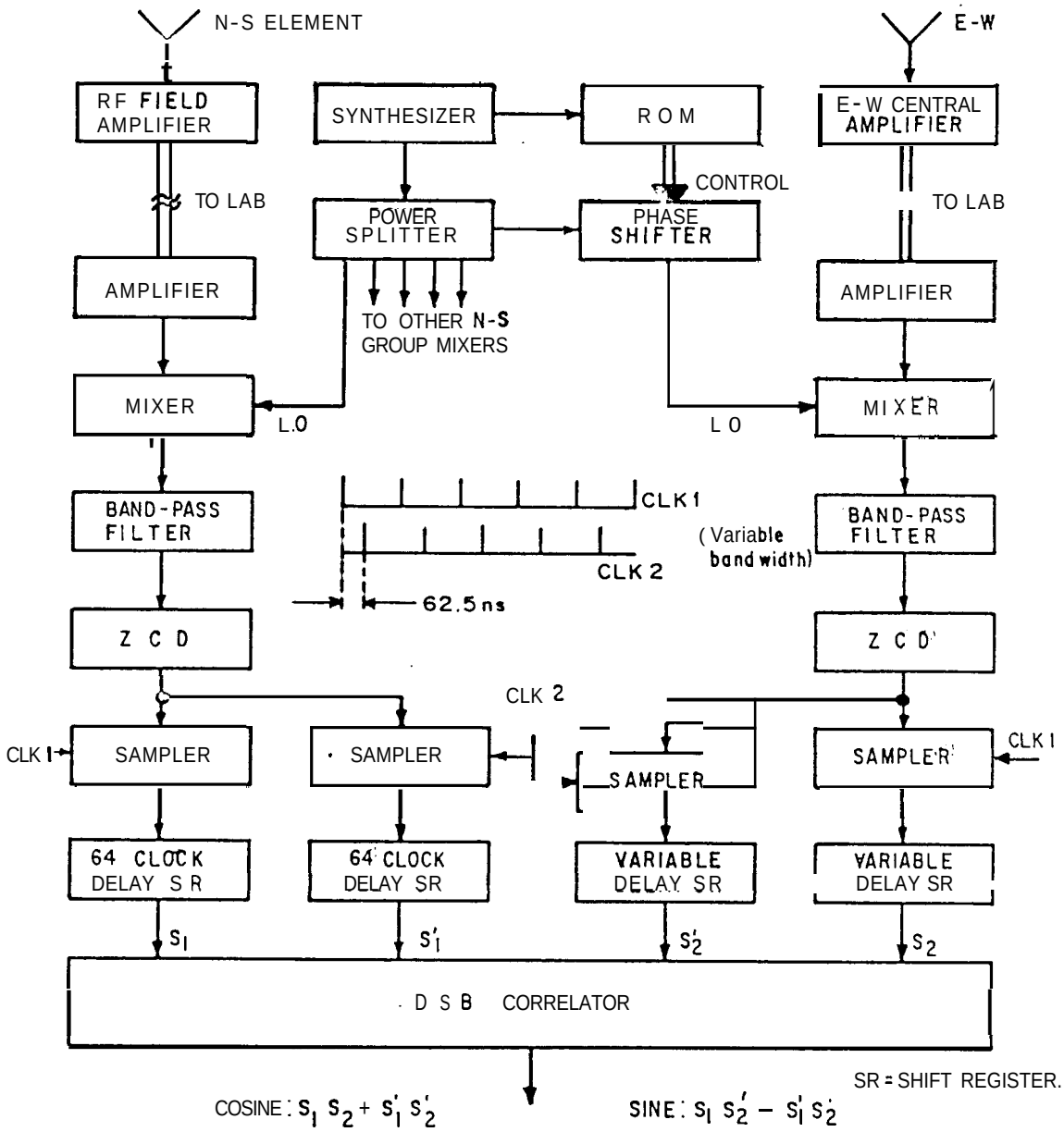

Fig. 2.7: Block diagram of the scheme used to obtain one of the visibilities.

employed to obtain the amplitude information (Fig. 2.8). As can be seen in this figure one uses a threshold detector instead of a zero cross detector. A suitable threshold value is that which is sensitive to the change in the area of the probability density function of the input signal. This value, V_{th}, is close to zero but should be well above the noise margin of the comparator. By varying this threshold value we also verified that the fluctuations of the input signal are indeed Gaussian in nature.

The receiver employs a double side band (DSB) system (Read 1963; Radhakrishnan et al. 1972) and uses clocks in quadrature to obtain the quadrature samples. In the present case, the I.F. bandwidth is 400 kHz. In the DSB technique this is further reduced by a factor of 2. However, this does not deteriorate the signal-to-noise ratio as we have two sets of 200 KHz signals which are in quadrature. The sampling fequency used is 2 MHz. With this over sampling the signal-to-noise ratio of the one-bit correlation coefficients improves from 64% to 80% of the analog correlation (Bowers and Klinger 1974).

Delay Adjustments

There is an excess delay in the EW signal corresponding to $\approx$1 km of cable length as compared to the signal from the southern elements (to recall, the EW singal travels through 1.5 km of cable length while the signal from any southern element travels only $\approx$ 0.5 km). A gross delay is included in the southern element signal path by a 64 clock pulse delay shift register (Fig. 2.7). Finer adjustments to obtain maximum correlation can be made using variable delay shift registers in the EW signal

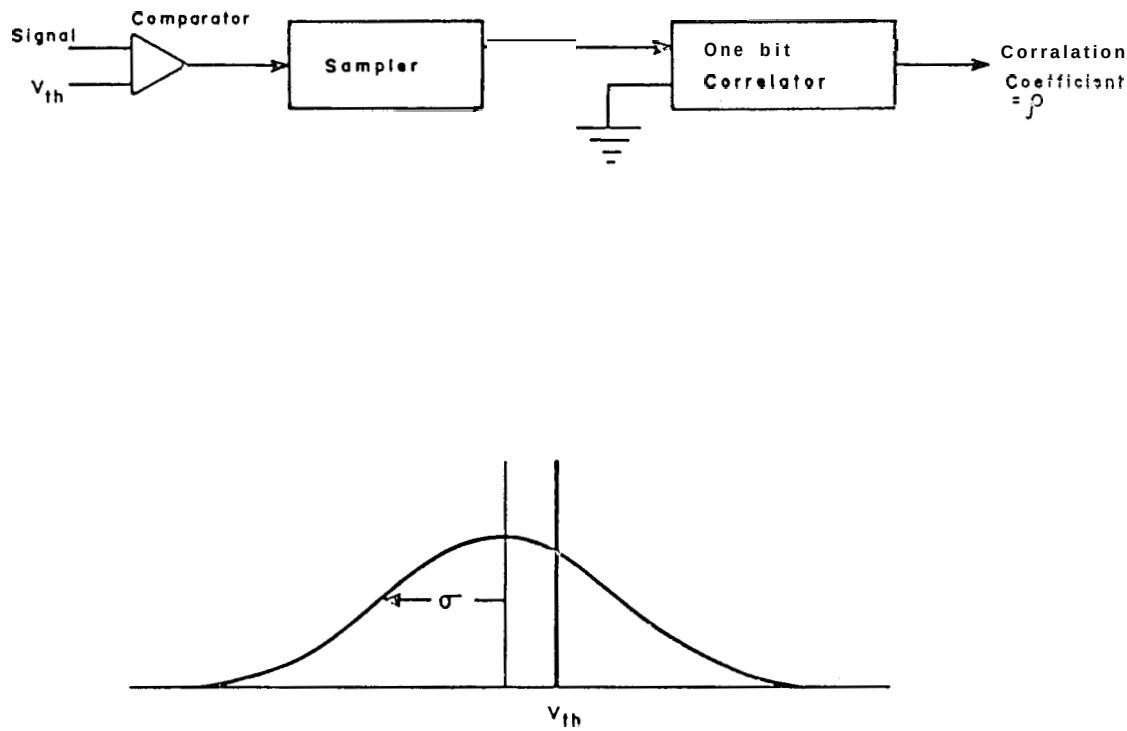

Fig. 2.8: The scheme used in the present observations to obtain the total power information using a one-bit correlator and a threshold detector. The probability, P, that the signal amplitude is less than a certain threshold V_{th} is given by:

$$P = \frac{1+\rho}{2} = \frac{1}{2} + \frac{1}{\sqrt{\pi}} \int_0^{V_{th}/\sqrt{2}\sigma} e^{-t^2} dt$$

path. Since one is using the DSB technique any phase corrections will be independent of the delay. A maximum error of $\pm 0.25\mu$ sec of delay will be left uncompensated due to the quantised nature of the delay settings. This leads to a maximum decorrelation of only 2% for 200 KHz bandwidth and is not serious.

2.3 RECEIVER PERFORMANCE

The digital receiver system has built in it a noise diode, a crystal oscillator and a 32-way power splitter which can be used for any system test. Desired levels of noise and/or continuous wave signal can be fed to the receiver system and the correlations can be recorded. For a correlated noise input the laboratory tests gave an average value of correlation coefficient of 98.8% in the 32 I.F. channels with a scatter whose r.m.s. is 0.4%. The average value is less than 100% due to the receiver noise and the non-ideal behaviour of the zero cross detectors and the correlators discussed below. The r.m.s. value indicates the differences in the 32 I.F. band shapes. The average and r.m.s. were found to be repeatable over large gaps of time.

2.3.1 The receiver offsets

These are offsets of the system and are undesirable while measuring the correlation due to the signals from the antenna. These offsets, which are additive to the true correlations measured, generate artefacts on the map. They can be estimated by measuring the correlation coefficient for two uncorrelated signals. They have to be then subtracted (provided they are not changing with time) from the measured correlation coefficients.

In the present case, the receiver offset has been estimated by feeding uncorrelated noise in the lab and averaging the receiver output for 15 minutes. The integration time was chosen such that it is considerably longer than the time for which the synthesis data is integrated (i.e. $\approx$ 24 sec). Subtraction of two such 15 minute averages leaves essentially a random pattern as a function of correlator numbers and has an r.m.s. of 0.6 $\times 10^{-4}$. That is the accuracy to which the receiver offsets have been estimated. This number translates to $<$ 0.5 Jy r.m.s. fluctuation in the map which as we shall see later in this chapter is smaller than other sources of noise present in the map.

A quantitative discussion of the origin of these offsets is beyond the scope of the present outline. We shall merely remark here that analyses carried out on the receiver offsets indicated that the correlators were behaving ideally and the origin of the offsets may, instead, be in the zero cross detectors (ZCDs) and the samplers used in the receiver (Fig. 2.7). A small but finite value of the 'zero' of the ZCD can result in the offsets we have seen.

2.4 ANTENNA PERFORMANCE

The antenna system used for the observations consists of one row in the EW arm, 1.4 km long and 90 rows in the southern arm, spaced over 0.45 km. In all, they contain $\approx$ 500 dipoles. Any of these dipoles and/or the subsequent amplifiers could misbehave due to a variety of reasons. In addition, in the EW array the signal travels through a 1.4 km long cabling system while the signal from the southern array elements are brought to the

laboratory through open wire transmission lines which are ≈ 500 m long. To make sure that the antenna performance is near ideal a variety of checks are made routinely and the approximate illumination patterns of the EW and S arrays are determined. These checks are made by feeding appropriate levels of noise or continuous wave signal to various stages in the antenna and measuring the output in the laboratory. The most effective way of checking was transmitting a continuous wave signal from a dipole and measuring the outputs from the adjacent dipoles in the antenna. This method was very useful in locating the faults in the dipoles in the antenna system which are difficult to probe by other means.

These checks give an approximate illumination pattern of the EW array and of the S array basic units. It was found to be uniform and stable within an r.m.s. of 1 dB and 5° in amplitude and phase. A detailed discussion of this based on the results obtained from point source observations is given in the next chapter.

2.4.1 Loss before the pre-amplifier and the pre-amplifier noise temperature

Consider any of the southern array elements, Each is a basic unit like the one shown in figure 2.2 followed by a pre-amplifier (F.E.T. amplifier). The minimum antenna temperature that the basic units see is25000 K. Compared to this, the pre-amplifier noise temperature of ≈ 500 K is small. If the output of the pre-amplifier is measured once with its input terminated by its characteristic impedence and then with the antenna connected

to the pre-amplifier, then a 10 dB increase in the power level is to be expected if losses before the pre-amplifier are neglected. Measurements made on the 88 rows of the southern array give an average value of 8 dB with an r.m.s. value of 1 dB. The major reason for the lower value of the signal-to-noise ratio is due to the small but finite loss of ≈ 1 dB before the pre-amplifier (Fig. 2.2). The r.m.s. value of 1 dB reflects the variations in the loss before the pre-amplifier and the variations in the amplifier noise temperature. This will contribute to a scatter in the recorded amplitudes of the visibilities which we shall discuss in the next chapter.

2.4.2 Gain variation of amplifiers

Since we have employed a one-bit correlator system, small variations in the gains of the amplifiers in the S array practically do not affect the measurement of the correlation coefficients. However, to obtain the amplitude information lost in one-bitting, we record the total powers from the single row of the EW array used for observation and from one of the southern array elements. Note that it is enough to measure the total power from any one representative row in the southern array, since all of them are similar and are looking into the same part of the sky. Total power measurements, surely, are affected by the gain variations of the amplifiers. Hence a check on this is needed.

A noise diode and a diode switch are introduced in the signal path of the III row of the East array and as well as of the West array, as shown schematically in Fig. 2.4. Control

signals from the laboratory disconnect the signal from the antenna and turn on the noise diode when required. The power output of the noise diode is adjusted to be equal to the typical power output of the antenna. After turning on the noise diode its output stabilizes in less than 1 sec and is constant with time to an accuracy of better than 1%.

During the observations, the noise diode is turned on once every hour and the output recorded for 24 sec. Of course, as can be seen from Fig. 2.4 this method of testing takes care of any gain variations in the christmas tree subsequent to the point at which the noise is introduced. We have introduced the noise diode before the two amplifiers whose gain variations can affect the final East or West array outputs, Variations in the gains of the amplifiers present before this stage can affect only a group or a part of a group in the array which is less serious for the total power measurements. In any case, introducing a noise diode and a switch before every pre-amplifier in the EW array would need 20 such units and has practical difficulties of implementation.

A similar arrangement was also made for the representative southern array element whose total power is measured.

The measurements made at the end of every hour implied no variation greater than +2% in the gains of the amplifiers.

2.4.3 Illumination pattern of the EW and S arrays

Illumination pattern of the aperture of an antenna is related to the far-field voltage radiation pattern of the antenna, f (l), by a fourier transform. For a linear array of

extent X wavelengths this relation is as follows:

$$f(l) = F_e(l) \sum_{-X/2}^{X/2} g(x)\, e^{-j2\pi x l}\, dx \qquad (2.4).$$

$g(x)$ which in this case represents the illumination pattern of the linear array is in general complex. $F_e(l)$ is the far-field pattern of the elements which comprise the array. For a uniformly illuminated aperture, the far-field pattern (beam) is $F_e(l)\ \mathrm{Sin}(\pi X l)/(\pi X l)$. Strong point sources can beobserved to record the beam of the EW antenna in time and by an inverse fourier transform obtain the illumination pattern on the EW antenna. The illumination pattern of the S array can be obtained by the visibilities recorded in the different baselines for strong point sources.

Non-uniform illumination pattern can change not only the beam shape of the antenna but also its gain. In the present case, if this happens in the EW antenna it will introduce an overall multiplication factor in the visibilities obtained with the southern array. On the other hand, a non-uniform illumination pattern over the 88 basic units in the southern array introduces a scatter in the observed visibilities. In the next chapter, we comment on what the point source observations tell us about the illumination patterns and their variations.

2.5 SENSITIVITY

The sensitivity of a telescope is a measure of the minimum signal it can detect. Even in the absence of any source of radiation in the sky the output of a telescope will not be

steady and will have fluctuations which correspond to the noise inherent to any such system. In general the amount of fluctuation expected can be quantified by,

$$\Delta T = M \frac{T_{SYS}}{\sqrt{Bt}} \qquad (2.5)$$

where, T_{SYS} is the system temperature ($= T_{SKY} + T_{RX}$),

T_{SKY} is the contribution due to the sky,

T_{RX} is the contribution from the receiver,

B is the bandwidth of the singal being analysed,

t is the integration time after which noise is looked at,

and M is the non-ideality factor (see Christiansen and Hogbom, 1985 for a general dicussion on sensitivity).

At low frequencies $\sim$ 30 MHz, T_{SYS} is almost entirely determined by the sky noise. This is contributed by the synchrotron background radiation which is produced by the relativistic electrons gyrating in the magnetic field of the Galaxy. One can associate an equivalent black body temperature with this radiation and this value varies depending on the frequency of observation and where one is looking in the sky. A typical antenna temperature encountered in Gauribidanur is $\approx 10^4$ K. Compared to this the first stage amplifiers in the antenna have a noise temperature of 500 K which is small. Thus, given a bandwidth of 400 kHz and an integration time of 10 sec (which are appropriate for the continuum observations described in this thesis), ΔT for $T_{SYS} = 10^4$ K will be 5 K for M = 1. This limit can be translated to minimum detectable flux for a point source as follows:

$$\Delta S = \frac{\frac{1}{2} k_B \Delta T}{A} = M \frac{3500}{A} \text{ Jy} \qquad (2.6)$$

where k_B is the Boltzmann constant (= 1.38 X 10^{-23} W Hz^{-1} K^{-1}) and A is the effective area of the telescope.

For a correlation receiver, $M = \sqrt{2}$ and the effective area $A = 2\sqrt{A_1 A_2}$ where A_1 and A_2 are the areas of the two antennas whose outputs are multiplied. For the single beam system which we mentioned in Chapter 1, $A \approx 18000$ m^2 and $\Delta s = 0.3$ Jy. This is the system sensitivity for point sources. We would now like to estimate the surveying sensitivity, $(\Delta s)_S$ of the single beam system. Suppose that all of the observable sky from Gauribidanur has to be mapped in a day's time using the single beam system. Within a given integration time there are 180 independent directions along NS which are to be observed to cover the complete sky along NS. So, the sensitivity of such a scheme will be $(\Delta s)_S = 0.3 \times \sqrt{180} = 4$ Jy. We estimate below the corresponding number for the present survey made using the synthesis technique.

In the present system, where we are using one-bit correlators, $M = \sqrt{2} \times \pi/2$. But, due to oversampling, this is brought down to $\sqrt{2} \times 1.25$ (Bowers and Klinger 1974). Also, in the present scheme of synthesis since we are using only one row of EW the collecting area of the EW array is lower by a factor of 4 as compared to the single beam system. In addition, since we are employing switching between every 4 units of the S array the effective integration time is lower by a factor of 4. With these factors $\Delta s = 1.5$ Jy - which is also the surveying sensitivity in

the present case.

There is another factor which is expected to be as important in determining the sensitivity of GEETEE for point source detection as the system noise, and that is confusion. This refers to the fact that given a certain solid angle one can find a flux level at which there is typically one source in it (statisticaly). If the solid angle is chosen to be the main beam of GEETEE, then, the flux level at which there is one source in it is around 3 Jy. To estimate this, in principle one needs a log(N) vs. log(S) relation at this frequency, where N is the number of sources per steradian whose flux is greater than S. However, the estimate for the confusion limit as 3 Jy is extrapolated from the log(N) vs. log(S) relation at 408 MHz given by Shaver and Pierre (1989). As will be seen in the subsequent chapters, the r.m.s. value of noise in the maps in regions far away (where the system temperature is $\approx 1.5 \times 10^4$ K) from the Galactic plane is actually 4 Jy. So, at its full resolution GEETEE is confusion limited at 4 Jy.

However, the discussion about confusion limit is relevant only to the detection of point sources. For extended sources, the system noise still determines the sensitivity. A more detailed discussion of confusion and system noise can be found in Chapter 4.

2.6 GRATING RESPONSE

The rows in the S array are spaced 5 □ apart while the wavelength of observation is 8.69 a. Hence, there will be grating response of the array beyond the zenith angle θ such

that,

$$\text{Sin}\,\theta = \left(\frac{\lambda}{d} + \text{Sin}\,\theta_o\right) \qquad (2.7)$$

where,

$d = 5$ m

$\lambda = 8.6956$ q

θ_o = the zenith angle that is aliased with θ.

Equation (2.7) implies that a grating lobe appears at $\theta_o = \mp 90^o$ when the main beam is at $\theta = \pm 47^\circ$ (Fig. 2.9) and at $\theta = \pm 60^\circ$, the two responses are equal. Thus, the regions where $47^\circ < |\theta| < 90^o$ are aliased. Due to the effect of the primary beam, the gains of both the EW row and each of the S array elements go to zero at $|\theta| = 90^\circ$. Hence, for the sky in the region $47^o < |\theta| < 50^\circ$ there is less than 10 % aliasing from the sky in the range $76^\circ < |\theta| < 90^\circ$. Thus, though the maps given in Chapter 4 go even beyond this zenith angle, caution should be exercised in interpreting the maps beyond the zenith angles of $\pm 50^\circ$. This corresponds to the maps beyond the declinations of -36° and $+64^\circ$.

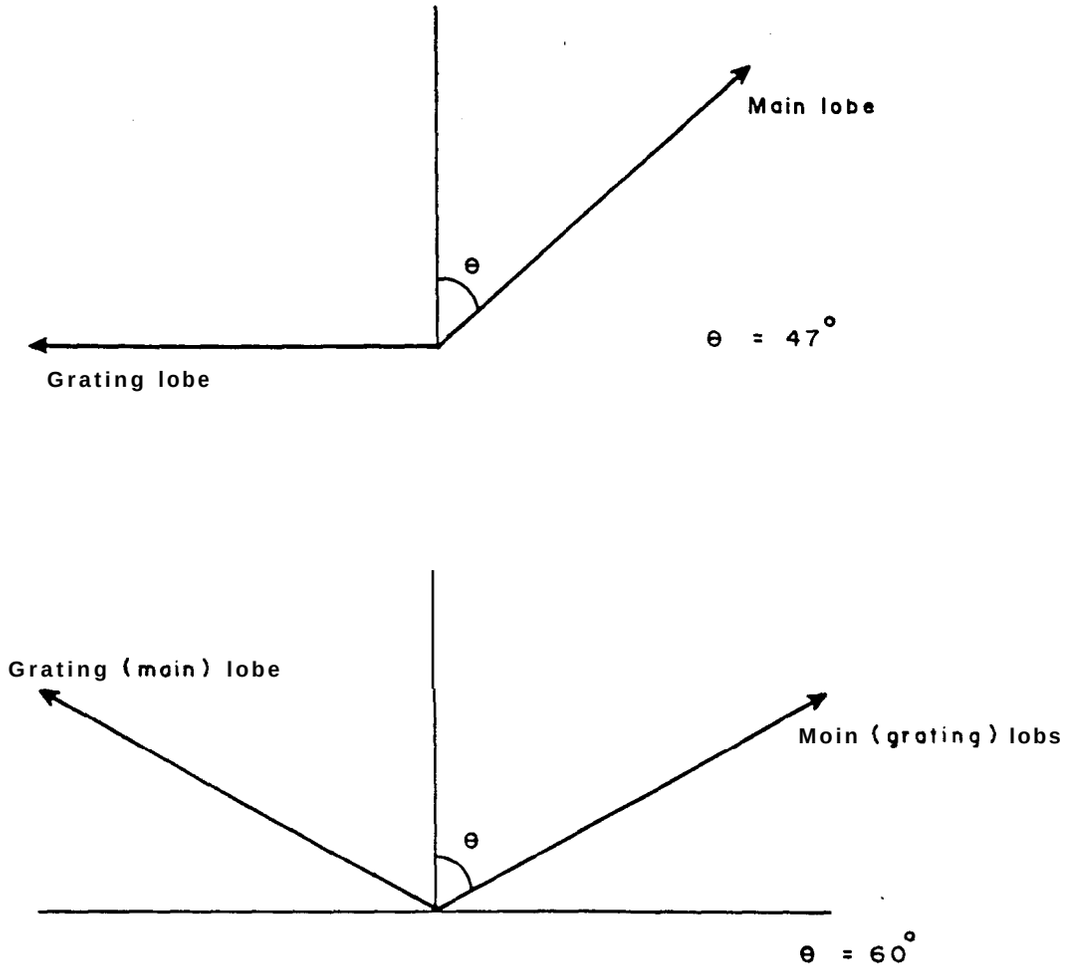

Fig. 2.9: This illustrates the grating response of GEETEE. When the main beam is pointed to $\pm 47^{o}$ of zenith angle, there is a grating response at $\mp 90^{o}$ of zenith angle. This grating response is heavily attenuated by the primary beam of the basic unit along NS. When the antenna beam is pointed to $+60^{o}$ the distinction between main beam and grating beam disappears. They have equal gains here. Sky between zenith angles of $\pm 47^{o}$ and $\pm 90^{o}$ is aliased.

REFERENCES

Bowers, F.K., Klinger, R.S. 1974, Astr. Astrophys. Supp. Ser.,15,373.

Christiansen, W.N., Hogbom, J.A. 1985, Radiotelescopes, Cambridge University Press.

Radhakrishnan, V., Brooks, J.W., Goss, W.M., Murray, J.D., Schwarz, U.J. 1972, Astrophys. J. Supp. Ser., 24, 1.

Read, R.B., 1963, Astrophys. J., 138,1.

Shaver, P.A., Pierre, M. 1989, ESO preprint, No. 637.

Udayashankar, N. 1986, Ph.D. Thesis, Dept. of Physics, Bangalore University, Bangalore.

van Vleck, J.H., Middleton, D. 1966, Proc. IEEE, 54, 2.